Electronic Supplementary Material (ESI) for Journal of Materials Chemistry C.

Evaluation of acenes as potential acceptors in thermally activated delayed fluorescence emitters and the promise of a phenoxazine-naphthalene emitter for OLEDs

Supporting information

Oliver S. Lee[a,b], Nidhi Sharma[a,b], Tomas Matulaitis[a], Alexandra M. Z. Slawin[a],Yoann Olivier[c], Ifor D. W. Samuel[b], Malte C. Gather[b,d*] and Eli Zysman-Colman[a*]

[a]Organic Semiconductor Centre, EaStCHEM School of Chemistry, University of St Andrews, St Andrews, UK, KY16 9ST

[b]Organic Semiconductor Centre, SUPA School of Physics and Astronomy, University of St Andrews, St Andrews, UK, KY16 9SS.

[c]Laboratory for Chemistry of novel materials, University of Mons-Hainaut, Place du Parc 20, B-7000 Mons, Belgium.

[d]Centre for NanoBioPhotonics, Department of Chemistry, University of Cologne, Greinstr. 4-6, 50939 Köln, Germany.

Table of Contents

1 Computations

1.1 Methodology

Density functional theory calculations were performed using the PBE0 functional,[1–3] 6-31G(d,p)[4–7] basis set and GD3BJ empirical dispersion,[8,9] with no solvation considered (gas phase). Each emitter first underwent a geometry optimisation calculation followed by a frequency calculation, to ensure the computed geometry was at a local minimum. The relaxed geometry was then used to calculate the first 10 singlet and 10 triplet vertical excited states of each emitter, using time-dependent DFT with the Tamm-Dancoff approximation (TDA).[10–13] All calculations were performed using Gaussian 16, revision C.01,[14] and all program defaults, except those noted above, were left as default for that program. All calculations were submitted and processed using in-house developed software, Silico ver 0,[15] which incorporates a number of publicly available software libraries, including: cclib[16] for parsing of result files, VMD[17]/Tachyon[18] for 3D rendering, Matplotlib[19] for drawing of graphs and Open Babel[20]/Pybel[21] for file interconversion.

1.2 Results

Table **S1**. Table of computational results from primary study.[a]

Name	HOMO /eV	LUMO /eV	Band Gap /eV	S_1 /eV	S_1 /nm	*f*	ΔE_{ST} /eV
1-Cz-Nap	-5.61	-1.22	4.39	3.57	347	0.03	0.66
1-DMAC-Nap	-5.11	-1.17	3.94	3.04	408	0.00	0.07
1-DMCz-Nap	-5.45	-1.32	4.13	3.26	380	0.00	0.32
1-DPA-Nap	-5.21	-1.01	4.20	3.43	362	0.12	0.70
1-DTBCz-Nap	-5.39	-1.17	4.22	3.43	362	0.04	0.55
1-PXZ-Nap	-4.91	-1.26	3.65	2.78	447	0.00	0.01
1,4-Cz-Nap-Cz	-5.65	-1.51	4.15	3.35	370	0.12	0.59
1,4-DMAC-Nap-DMAC	-5.21	-1.42	3.80	2.90	428	0.00	0.01
1,4-DMCz-Nap-DMCz	-5.61	-1.68	3.93	3.06	405	0.00	0.21
1,4-DPA-Nap-DPA	-5.03	-1.14	3.88	3.14	394	0.29	0.66
1,4-DTBCz-Nap-DTBCz	-5.40	-1.40	4.00	3.22	385	0.14	0.49
1,4-PXZ-Nap-PXZ	-5.05	-1.58	3.46	2.59	479	0.00	0.01
1,4-Cz-Nap-TRZ	-5.67	-2.00	3.67	3.03	410	0.16	0.47
1,4-DMAC-Nap-TRZ	-5.16	-1.98	3.18	2.45	505	0.00	0.01
1,4-DMCz-Nap-TRZ	-5.49	-2.07	3.42	2.70	458	0.00	0.07
1,4-DPA-Nap-TRZ	-5.33	-1.83	3.50	2.93	423	0.45	0.61
1,4-DTBCz-Nap-TRZ	-5.46	-1.96	3.50	2.88	431	0.19	0.38
1,4-PXZ-Nap-TRZ	-4.94	-2.04	2.91	2.20	564	0.00	0.01
2-Cz-Nap	-5.57	-1.18	4.39	3.69	336	0.10	0.77
2-DMAC-Nap	-5.08	-1.19	3.90	3.09	402	0.00	0.07
2-DMCz-Nap	-5.43	-1.31	4.12	3.33	372	0.00	0.33
2-DPA-Nap	-5.15	-0.90	4.24	3.57	347	0.12	0.81
2-DTBCz-Nap	-5.36	-1.12	4.24	3.57	348	0.11	0.67
2-PXZ-Nap	-4.90	-1.25	3.66	2.87	433	0.00	0.06
2,6-Cz-Nap-Cz	-5.54	-1.43	4.11	3.44	360	0.24	0.65

2,6-DMAC-Nap-DMAC	-5.18	-1.45	3.73	2.93	423	0.00	0.03
2,6-DMCz-Nap-DMCz	-5.57	-1.67	3.90	3.13	396	0.00	0.16
2,6-DPA-Nap-DPA	-4.86	-0.97	3.90	3.27	380	0.30	0.73
2,6-DTBCz-Nap-DTBCz	-5.30	-1.32	3.99	3.33	373	0.29	0.58
2,6-PXZ-Nap-PXZ	-5.03	-1.56	3.47	2.70	459	0.00	0.04
2,6-Cz-Nap-TRZ	-5.64	-1.97	3.67	3.17	391	0.41	0.53
2,6-DMAC-Nap-TRZ	-5.13	-2.00	3.14	2.55	486	0.00	0.01
2,6-DMCz-Nap-TRZ	-5.47	-2.07	3.40	2.82	439	0.00	0.06
2,6-DPA-Nap-TRZ	-5.27	-1.76	3.51	3.06	405	0.67	0.62
2,6-DTBCz-Nap-TRZ	-5.44	-1.93	3.50	3.03	410	0.43	0.44
2,6-PXZ-Nap-TRZ	-4.95	-2.04	2.91	2.34	530	0.00	0.01

[a] Computations performed at the TDA/PBE0/6-31G(d,p)/GD3BJ level of theory. Excited states were calculated as vertical transitions.

Table **S2**. Table of computational results from the acene study.[a]

Name	HOMO /eV	LUMO /eV	Band Gap /eV	S_1 /eV	S_1 /nm	*f*	ΔE_{ST} /eV
1,4-PXZ-Ph-PXZ	-5.00	-0.84	4.17	3.20	388	0.00	0.21
1,4-PXZ-Nap-PXZ	-5.05	-1.58	3.46	2.59	479	0.00	0.01
1,4-PXZ-Anth-PXZ	-5.05	-2.07	2.98	2.18	569	0.00	0.14
9,10-PXZ-Anth-PXZ	-5.01	-2.15	2.86	2.02	613	0.00	0.03
1,4-PXZ-Tetra-PXZ	-5.04	-2.41	2.63	1.90	651	0.00	0.49
5,12-PXZ-Tetra-PXZ	-5.01	-2.50	2.52	1.73	719	0.00	0.35
1,4-PXZ-Penta-PXZ	-5.04	-2.66	2.38	1.72	722	0.00	0.76
5,14-PXZ-Penta-PXZ	-5.01	-2.73	2.28	1.53	808	0.00	0.60
6,13-PXZ-Penta-PXZ	-4.99	-2.77	2.22	1.45	853	0.00	0.53
1,4-PXZ-Hexa-PXZ	-4.85	-2.84	2.01	1.59	781	0.00	0.96
5,16-PXZ-Hexa-PXZ	-4.88	-2.90	1.99	1.41	880	0.00	0.80
6,15-PXZ-Hexa-PXZ	-4.93	-2.95	1.98	1.30	955	0.00	0.70

[a] Computations performed at the TDA/PBE0/6-31G(d,p)/GD3BJ level of theory. Excited states were calculated as vertical transitions.

Table **S3**. Table of computed relaxed excited states.[a]

Name	S_1 /eV	S_1 /nm	*f*
2-PXZ-Nap	2.30	539	< 0.0
1-PXZ-Nap	2.21	561	< 0.0
1,4-PXZ-Nap-PXZ	2.04	609	< 0.0

[a] Computations performed at the TDA/PBE0/6-31G(d,p)/GD3BJ level of theory. Excited states were calculated as vertical transitions.

Table **S4**. Table of computed S_1 and T_1 energies in DCM and toluene.[a]

	Toluene				DCM			
Name	S_1 /eV	T_1 /eV	ΔE_{ST} / eV	H_{SO} /cm^{-1}	S_1 /eV	T_1 /eV	ΔE_{ST} / eV	H_{SO} /cm^{-1}
2-PXZ-Nap	2.98	2.90	0.08	0.36	3.07	2.95	0.11	0.48
1-PXZ-Nap	2.87	2.86	0.01	0.05	2.95	2.93	0.01	0.08
1,4-PXZ-Nap-PXZ	2.66	2.64	0.01	< 0.01	2.71	2.70	0.01	< 0.01

[a] Computations performed at TDA/PBE0/6-31G(d,p)/ GD3BJ level of theory, using the IEFPCM implicit solvent model. Excited states were calculated vertically, using ground state geometries optimised in the given solvent.

1.3 LUMO Densities of Pentacene Derivatives

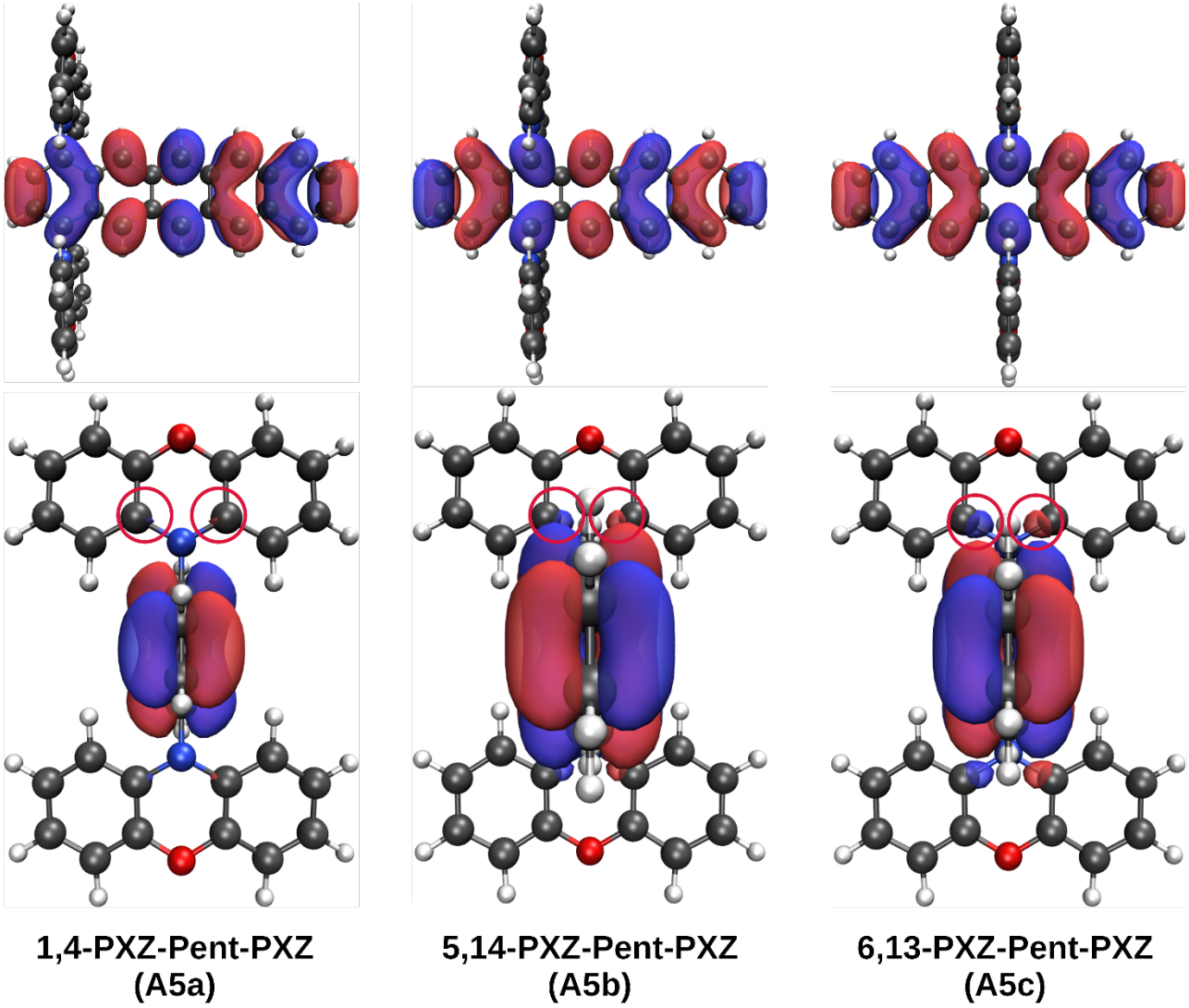

Figure **S1**. LUMO densities of the pentacene derivatives (isovalue = 0.02), highlighting the change in coefficient on the phenoxazine donor as the substitution pattern changes.

2 Synthesis

2.1 General Considerations

Reagents and solvents were purchased from commercial sources and used without prior purification, except for phenoxazine, which was purified by column chromatography in 5 vol% EtOAc/Hexane. Solvents (where noted) were degassed *via* a 3-cycle freeze-pump-thaw method. Flash column chromatography was performed using silica gel (Silia-P from Silicycle, 60 Å, 40-63 µm). Analytical thin-layer chromatography (TLC) was performed using pre-coated silica plates (silica gel 60) with

fluorescence indicator UV_{254}, and compounds were visualised under 254 or 365 nm UV-light. ^{1}H and ^{13}C NMR spectroscopy was performed on a Bruker Avance 400 MHz spectrometer, and peak shifts are assigned relative to the residual solvent peak. High resolution mass spectrometry (HRMS) was performed by the EPSRC National Mass Spectrometry Service Centre (NMSSC), Swansea University. Melting points were obtained using an Electrothermal Mel-Temp™ digital melting point apparatus in open-ended capillary tubes and are uncorrected. Gas-chromatography mass-spectrometry (GCMS) was performed using a Shimadzu GCMS QP2010 SE instrument. dba = dibenzylideneacetone, XPhos = 2-Dicyclohexylphosphino-2′,4′,6′-triisopropylbiphenyl.

2.2 2-(10-phenoxazinyl)naphthalene (2-PXZ-Nap)

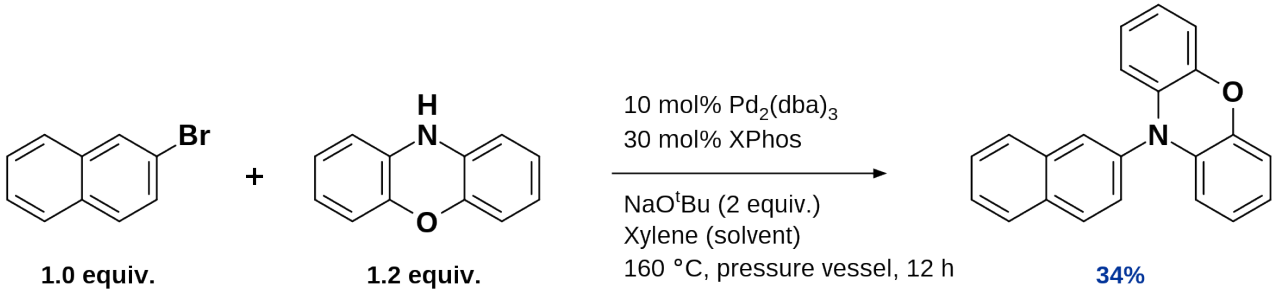

Figure **S2**. Synthesis of **2-PXZ-Nap**.

2-bromonaphthalene (1.00 g, 4.83 mmol, 1.00 equiv.), 10H-phenoxazine (1.060 g, 5.79 mmol, 1.20 equiv.), tris(dibenzylideneacetone)dipalladium(0), $Pd_2(dba)_3$, (0.442 g, 0.48 mmol, 0.10 equiv.), 2-dicyclohexylphosphino-2′,4′,6′-triisopropylbiphenyl (XPhos) (0.690 g, 1.45 mmol, 0.25 equiv.) and sodium *tert*-butoxide (0.928 g, 9.66 mmol, 2.00 equiv.) were combined in a glass sided pressure vessel. Dry xylene (15.0 mL) was then added before the vessel was degassed by bubbling with N_2 for 15 min. The vessel was then sealed and heated to 160 °C for 12 h. After being allowed to cool to room temperature the crude reaction mixture was filtered through a silica pad before the xylene was removed under reduced pressure. The crude was then dissolved in DCM before being extracted from DCM/water. The aqueous layer was discarded, and the crude was analysed by thin-layer chromatography (TLC) in 10 vol% EtOAc/hexane. The crude mixture was then purified by column chromatography in 2 vol% EtOAc/hexane. The fractions containing the product were combined and the product was allowed to form as a precipitate. The precipitate was filtered to **yield** a silvery powder (0.500 g, 34%). **R_f:** 0.67 (10 vol% EtOAc/Hexane). **Mp.** 209 - 210 °C. **^{1}H NMR (500.1 MHz; CD_2Cl_2) δ_H (ppm)**: 5.99 (d, J = 7.9 Hz, 2H), 6.40 - 6.92 (m, 6H), 7.45 (dd, J = 8.6, 2.1 Hz, 1H), 7.62 (pd, J = 7.1, 1.6 Hz, 2H), 7.89 - 7.97 (m, 2H), 7.97 - 8.04 (d, J = 7.8 Hz, 1H) and 8.14 (d, J = 8.6 Hz, 1H). **^{13}C NMR (127.8 MHz; DMSO-d_6) δ_C (ppm):** 113.9 (CH), 115.8 (CH), 122.0 (CH), 124.2 (CH), 127.1 (CH), 127.5 (CH), 128.1 (CH), 128.3 (CH), 128.4 (CH), 130.1 (CH), 132.0 (CH), 133.0 (C), 134.4 (C), 134.9 (C), 136.1 (C), 143.6 (C). **GCMS (11.96 min):** 309 ($[M]^+$).

2.3 1-(10-phenoxazinyl)naphthalene (1-PXZ-Nap)

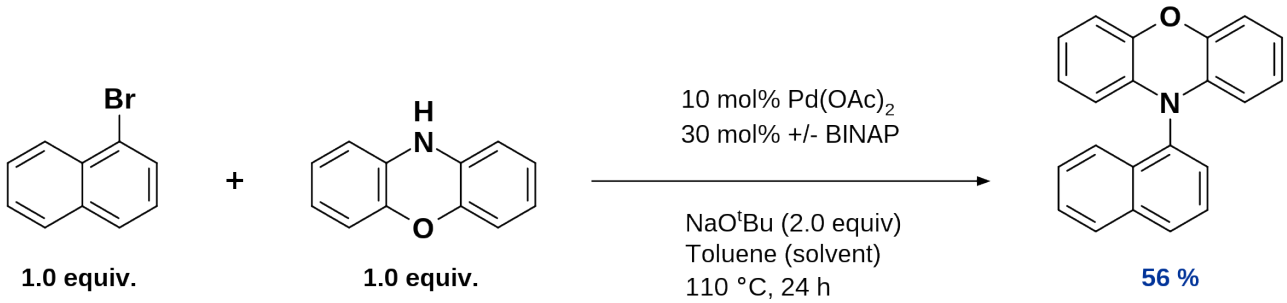

Figure **S3**. Synthesis of **1-PXZ-Nap**.

Sodium *tert*-butoxide (0.216 g, 1.93 mmol, 2.00 equiv.) was first loaded into a 2-necked round-bottomed flask before being degassed under vacuum for 15 min. The flask was then backfilled with N_2 before 1-bromonaphthalene (0.200 g, 0.97 mmol, 1.00 equiv.), 10H-phenoxazine (0.177 g, 0.97 mmol, 1.00 equiv.), palladium(II) acetate (0.021 g, 0.09 mmol, 0.10 equiv.) and +/- 2,2′-bis(diphenylphosphino)-1,1′-binaphthyl (+/- BINAP) (0.180 g, 0.29 mmol, 0.30 equiv.) were also added to the flask. Dry toluene (5.0 mL) was then added to the flask before the reaction was heated to 110 °C for 24 h. After being allowed to cool to room temperature, the crude was extracted from DCM/water and the solvent was evaporated under reduced pressure. The crude was then analysed by TLC in 5 vol% EtOAc/hexane before being purified by column chromatography in pure hexane. The fractions containing the product were combined and the solvent was removed to **yield** the product as a white powder (0.167 g, 56%). **R_f:** 0.56 (5 vol% EtOAc/Hexane). **Mp.** 194 - 195 °C. **^{1}H NMR (500.1 MHz; CD_2Cl_2) δ_H (ppm):** 5.73 (d, J = 8.0 Hz, 2H), 6.52 (t, J = 7.6 Hz, 2H), 6.66 (br-s, 1H), 6.76 (dd, J = 7.9, 1.5 Hz, 2H), 7.52 (ddd, J = 8.3, 6.9, 1.4 Hz, 1H), 7.57 - 7.62 (m, 2H), 7.72 (t, J = 7.8 Hz, 1H) and 8.01 - 8.12 (m, 3H). **^{13}C NMR (125.8 MHz; CD_2Cl_2) δ_C (ppm):** 115.2, 117.2, 123.2, 125.0, 125.3, 128.7, 128.8, 129.1, 130.7, 131.0, 131.1, 133.1, 136.2, 136.7, 137.6 and 145.8. **GCMS (11.38 min):** 309 ($[M]^+$).

2.4 1,4-di-(10-phenoxazinyl)naphthalene (1,4-PXZ-Nap-PXZ)

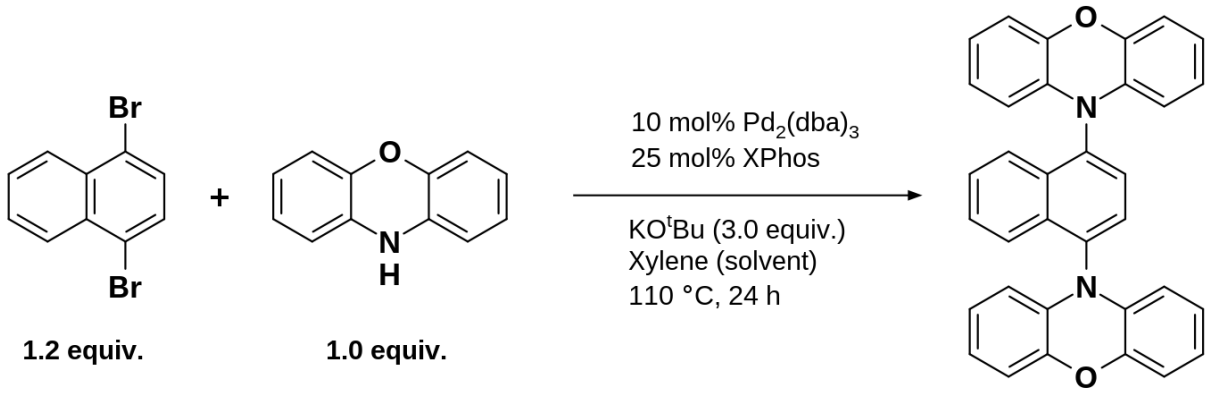

Figure **S4**. Synthesis of **1,4-PXZ-Nap-PXZ**.

$Pd_2(dba)_3$ (0.110 g, 0.11 mmol, 0.10 equiv.) and XPhos (0.143 g, 0.30 mmol, 0.25 equiv.) were combined, degassed under vacuum for *ca.* 30 min before being backfilled with N_2. Degassed xylene (mixture of isomers, 5.0 mL) was then added, and the resulting solution was heated to 90 °C. In a separate vessel, 1,4-dibromonaphthalene (0.412 g, 1.44 mmol, 1.2 equiv.), 10H-phenoxazine (0.220 g, 1.20 mmol, 1.0 equiv.) and KO^{t}Bu (0.404 g, 3.60 mmol, 3.0 equiv.) were combined, degassed under vacuum for *ca.* 30 min and likewise backfilled with N_2 (an excess of 1,4-dibromonaphthalene was found to be beneficial for the yield of this reaction despite the expected reaction stoichiometry, suggesting potential poisoning of the catalyst by phenoxazine at high concentrations). This solution was then transferred to the catalyst solution via cannula. To the remaining residue was added a further portion of degassed xylene (5.0 mL) which was gently warmed before also being transferred to the catalyst solution via cannula. The reaction was then heated to 110 °C for 24 h, before being allowed to cool back to room temperature. The xylene was then evaporated under reduced pressure. The resulting black solid was dissolved in DCM, filtered through a celite plug, extracted from DCM/H_2O, dried over $MgSO_4$ and then filtered. The crude was then analysed by TLC in 40 vol% DCM/hexane before being purified by column chromatography in DCM/hexane. Finally, the crude solid was recrystallised from DCM/MeOH to **yield** small, yellow crystals (0.090 g, 31%). **R_f:** 0.64 (40 vol% DCM/Hexane). **Mp.** 342 - 343 °C. **^{1}H NMR (400.1 MHz; $CDCl_3$) δ_H (ppm):** 5.81 (dd, *J* = 8.0 Hz, 1.5 Hz, 4H), 6.61 (td, *J* = 7.7, 1.5 Hz, 4H), 6.71 (td, *J* = 7.7, 1.5 Hz, 4H), 6.80 (dd, *J* = 8.0, 1.5 Hz, 4H), 7.56 (dd, *J* = 6.5, 3.2 Hz, 2H), 7.77 (s, 2H), 8.22 (dd, *J* = 6.5, 3.2 Hz, 2H). **^{13}C NMR (125.8 MHz; $CDCl_3$) δ_C (ppm):** 113.3 (CH), 115.7 (CH), 121.7 (CH), 123.5 (CH), 124.5 (CH), 128.3 (CH), 130.2 (CH), 133.6 (C), 134.0 (C), 136.0 (C) and 143.9 (C). **HR-MS (Xevo G2-S QToF): $[M+H]^+$ Calculated:** ($C_{34}H_{22}N_2O_2H$) 491.1760 **Found:** 491.1760. **GCMS (18.96 min):** 490 ($[M]^+$).

3 Electrochemistry

Cyclic Voltammetry (CV) and Differential pulse voltammetry (DPV) were performed on an Electrochemical Analyzer potentiostat model 620E from CH Instruments. CV was performed using a sweep rate of 100 mVs^{-1}. DPV was performed with an increment potential of 0.004 V, a pulse amplitude of 50 mV, a width of 0.05, and period of 0.5 s. Samples were prepared in acetonitrile (MeCN) solutions which were sufficiently purged with MeCN saturated N_2 so the O_2 peak could no longer be observed (approx. 15 minutes). All cells used 0.1 M MeCN solutions of tetra-n-butylammonium hexafluorophosphate ([^{n}Bu4N]PF6]) as the electrolyte, a glassy carbon working electrode, a Ag/Ag^+ reference electrode, and a platinum wide counter electrode. The redox potentials are reported relative to a saturated calomel electrode (SCE) with a ferrocene/ferrocenium (Fc/Fc^+) redox couple as the internal standard (0.45 V vs SCE).[22]

4 Photoluminescence Quantum Yields

Photoluminescence quantum yields for solutions were determined using the optically dilute method[23] in which four sample solutions with absorbances of ca. 0.10, 0.075, 0.050 and 0.025 at 360 nm were used. The Beer-Lambert law was found to remain linear at the concentrations of the solutions. For each sample, linearity between absorption and emission intensity was verified through linear regression analysis with the Pearson regression factor (R^2) for the linear fit of the data set surpassing 0.9. Individual relative quantum yield values were calculated for each solution and the values reported represent the slope obtained from the linear fit of these results. The quantum yield of the sample, Φ_{PL}, can be determined by equation **S1**.[23]

$$\Phi_{PL} = \Phi_r \frac{A_r}{A_s} \frac{I_s}{I_r} \frac{n_s^2}{n_r^2} \qquad \text{Equation } \mathbf{S1}$$

Where A = absorbance at the excitation wavelength (λ_{exc}: 360 nm), I = the integrated area under the emission curve, and n = the refractive index of the solvent. The subscripts '*s*' and '*r*' represent the sample and reference respectively. Φ_r = the absolute quantum yield of the external reference quinine sulfate (Φ_r = 54.6% in 1 M H_2SO_4).[23]

5 NMR Spectra

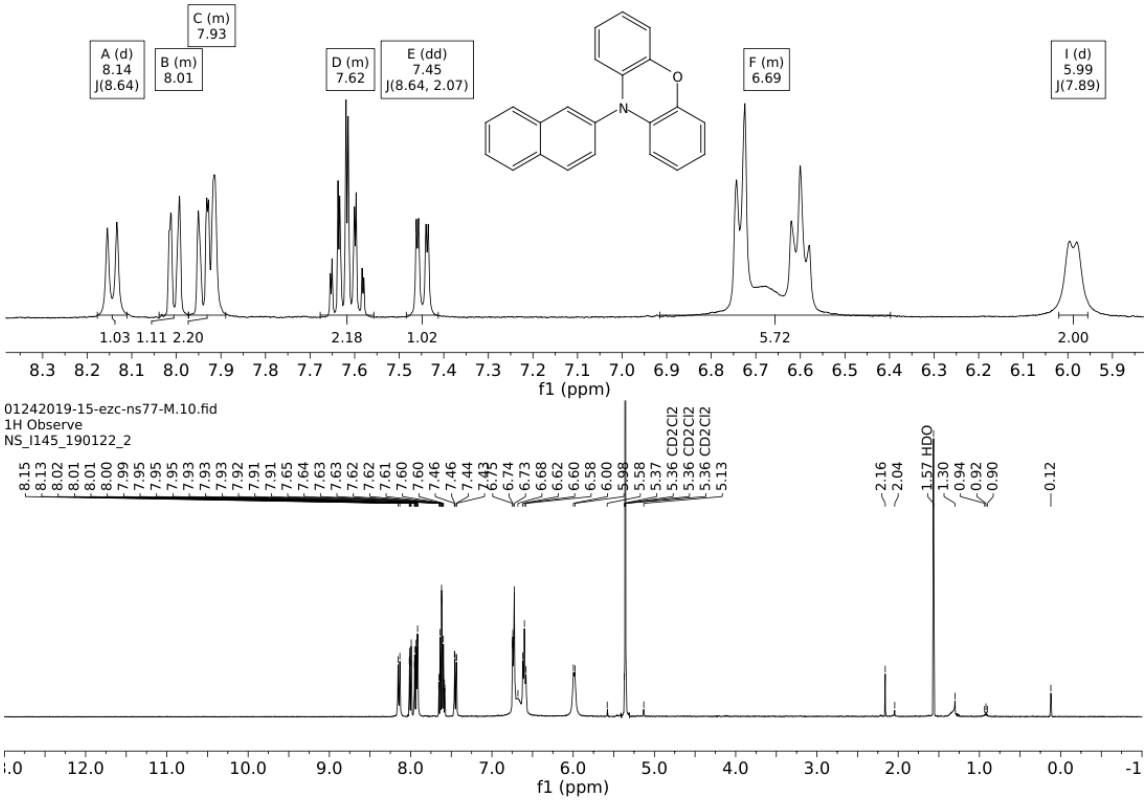

Figure **S5**. ^{1}H NMR of **2-PXZ-NAP** in $CDCL_3$

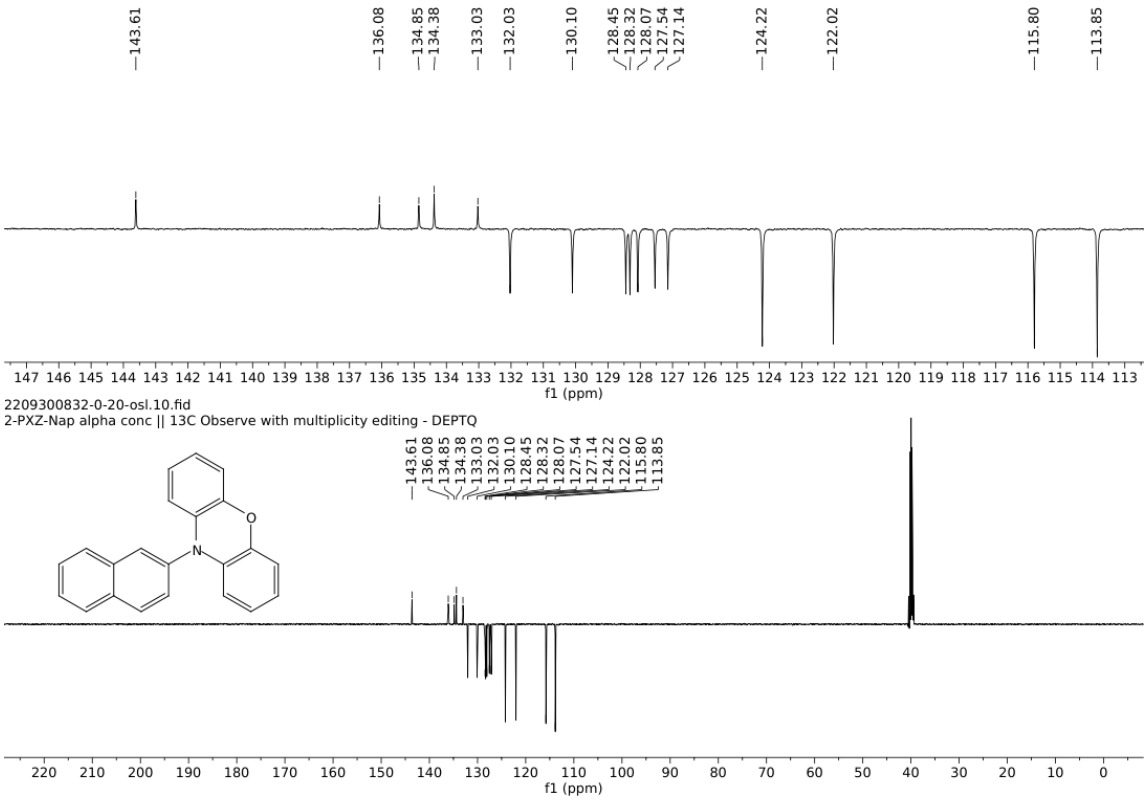

Figure **S6**. ^{13}C NMR of **2-PXZ-NAP** in $CDCl_3$

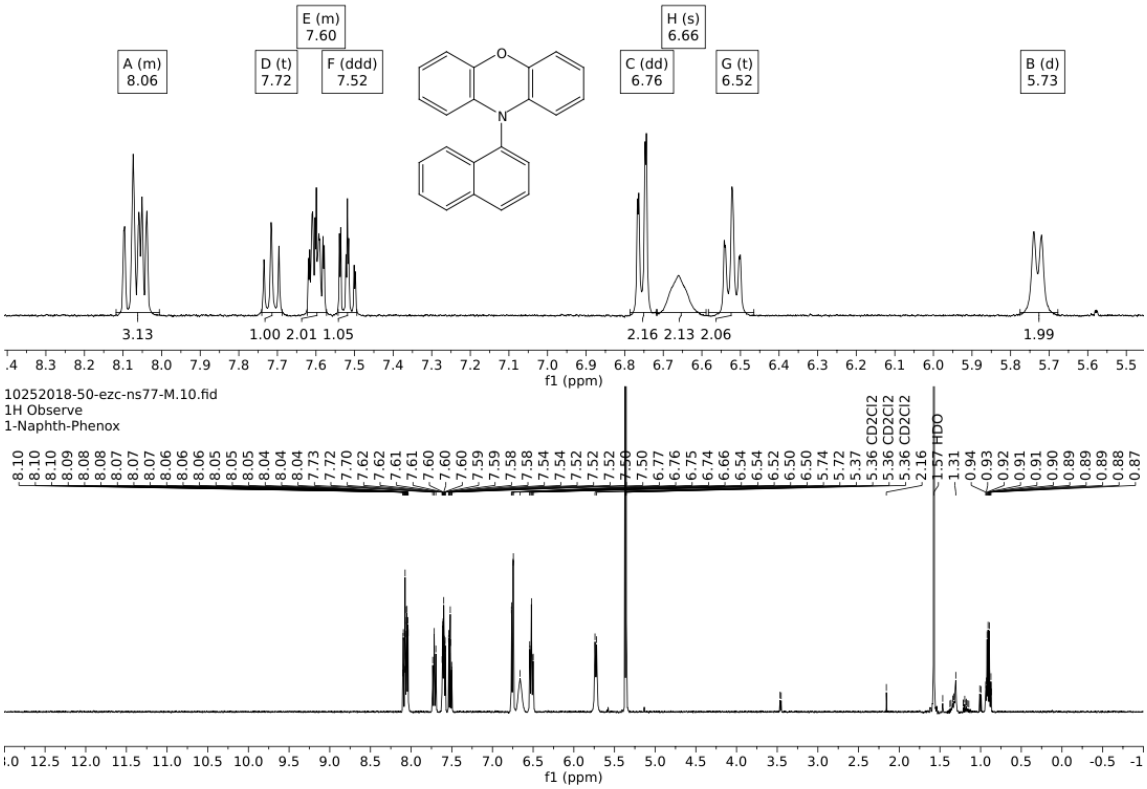

Figure **S7**. ^{1}H NMR of **1-PXZ-Nap** in $CDCl_3$

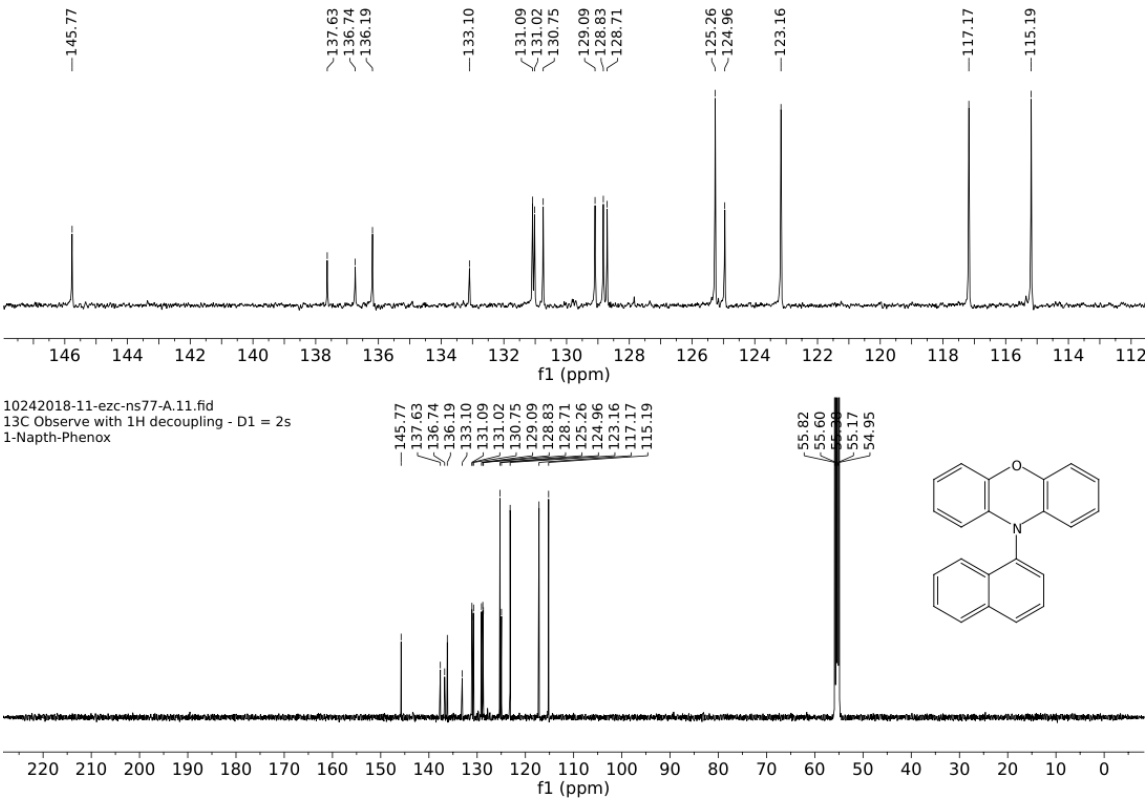

Figure **S8**. ^{13}C NMR of **1-PXZ-Nap** in CDCl3

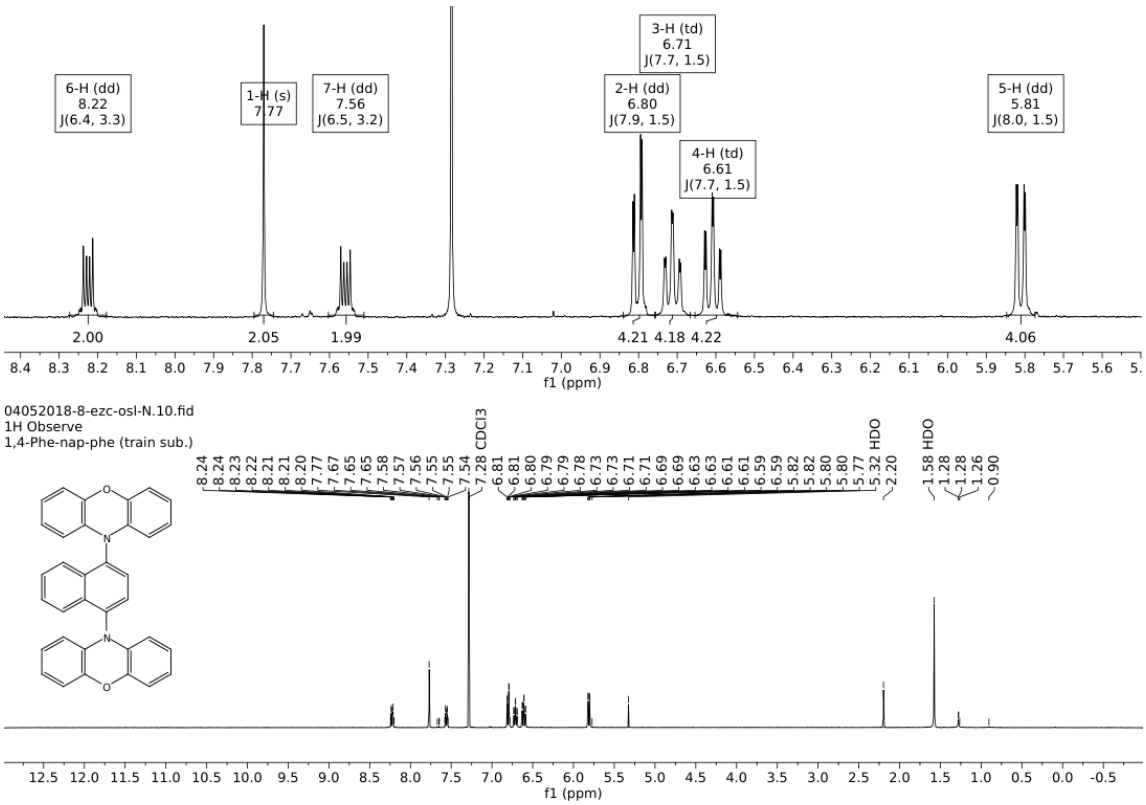

Figure **S9**. ^{1}H NMR of **1,4-PXZ-Nap-PXZ** in $CDCl_3$

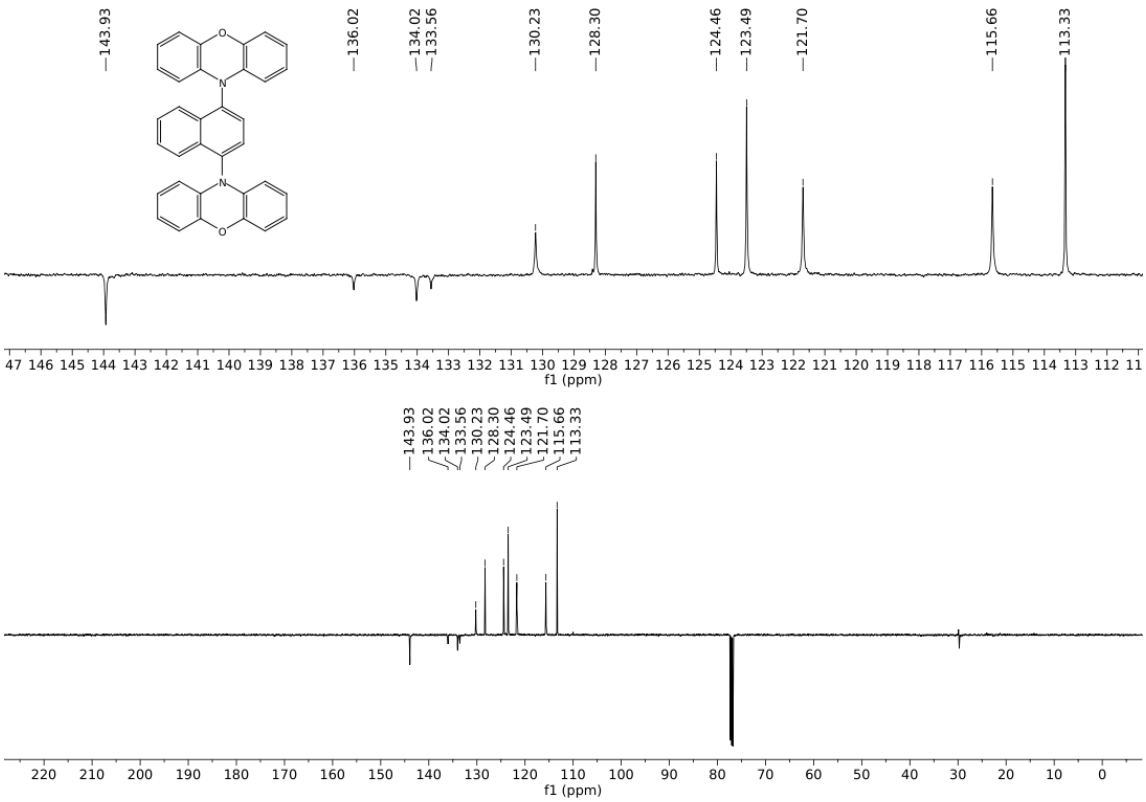

Figure **S10**. ^{13}C NMR of **1,4-PXZ-Nap-PXZ** in $CDCl_3$

6 HRMS Analysis

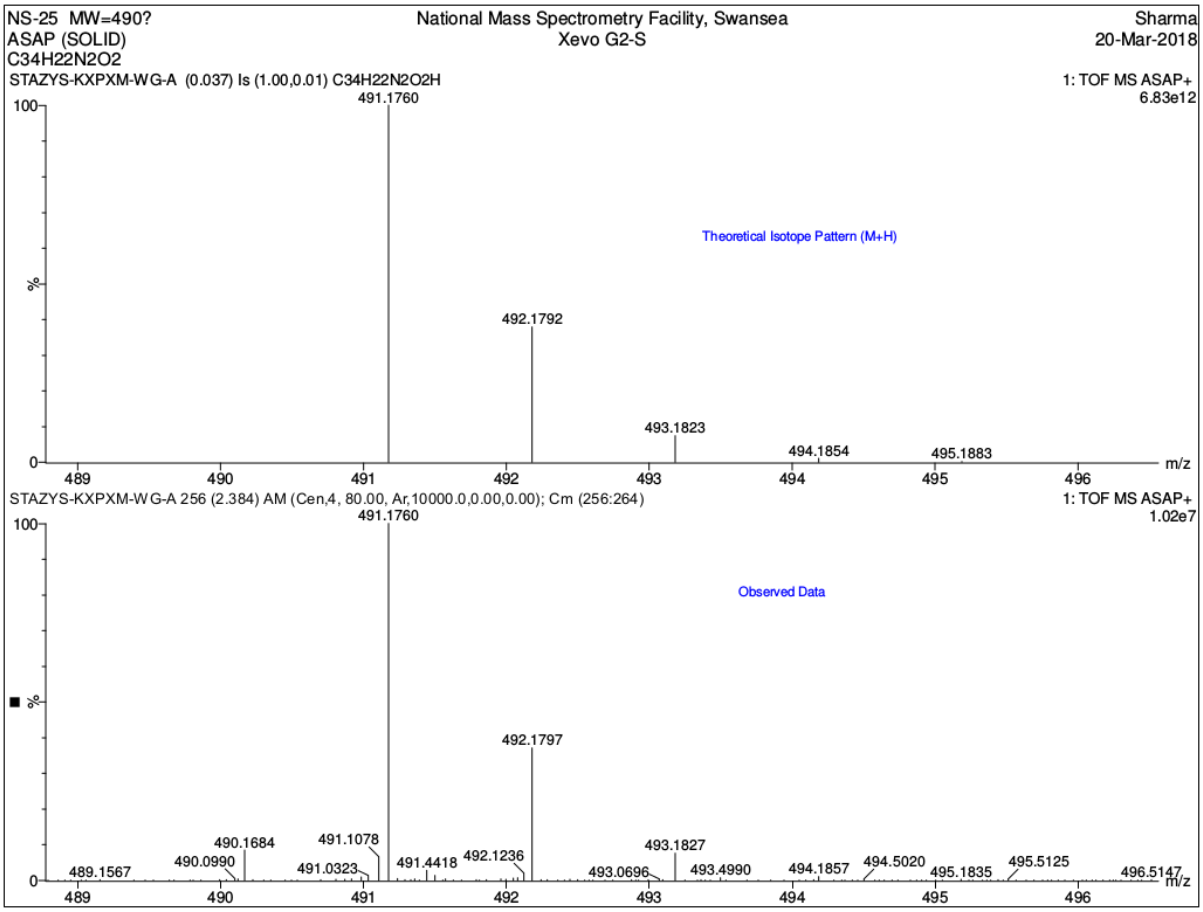

Figure **S11**. HRMS of **1,4-PXZ-Nap-PXZ**

7 GCMS Analysis

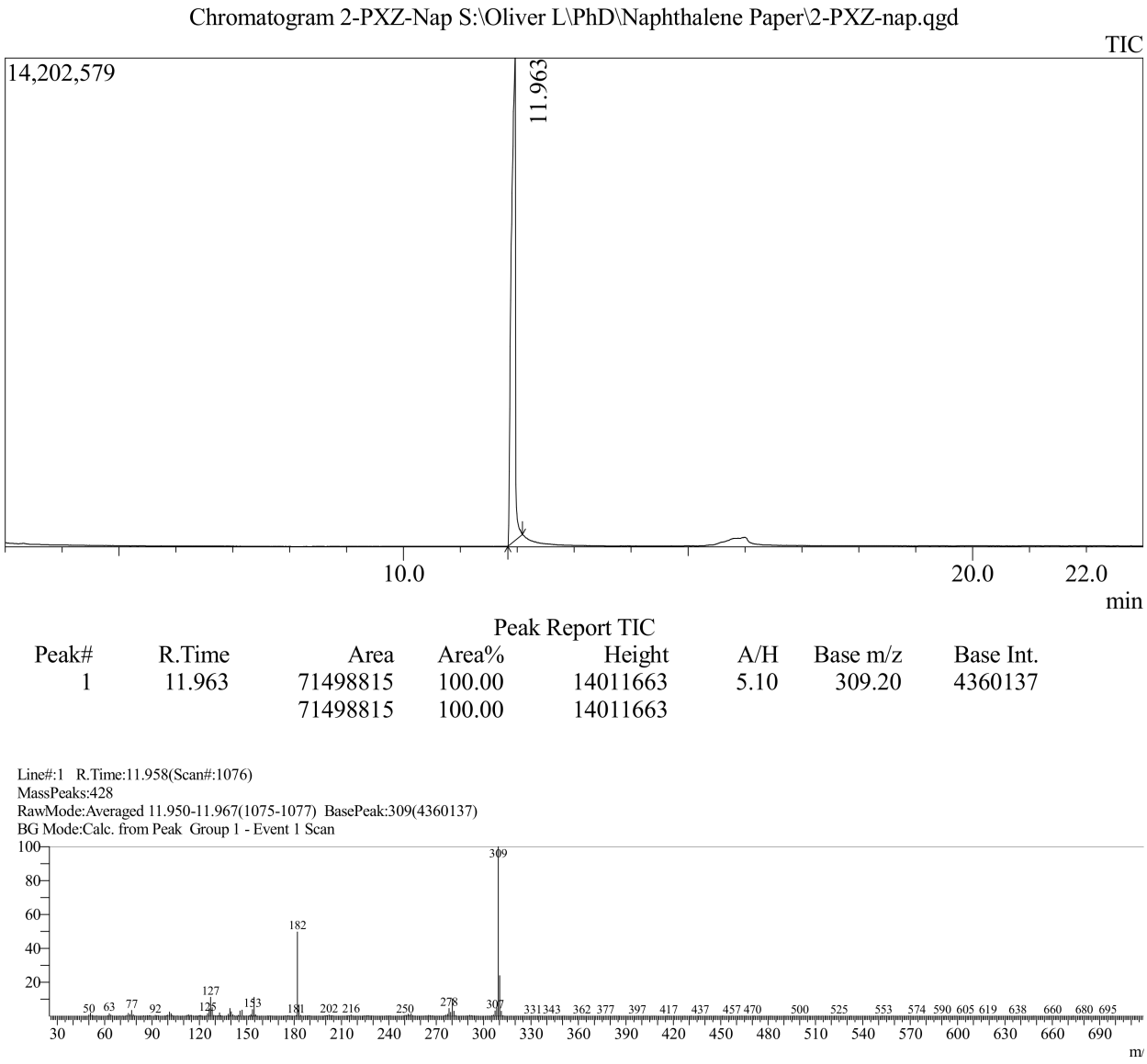

Figure **S12**. GCMS of **2-PXZ-Nap**

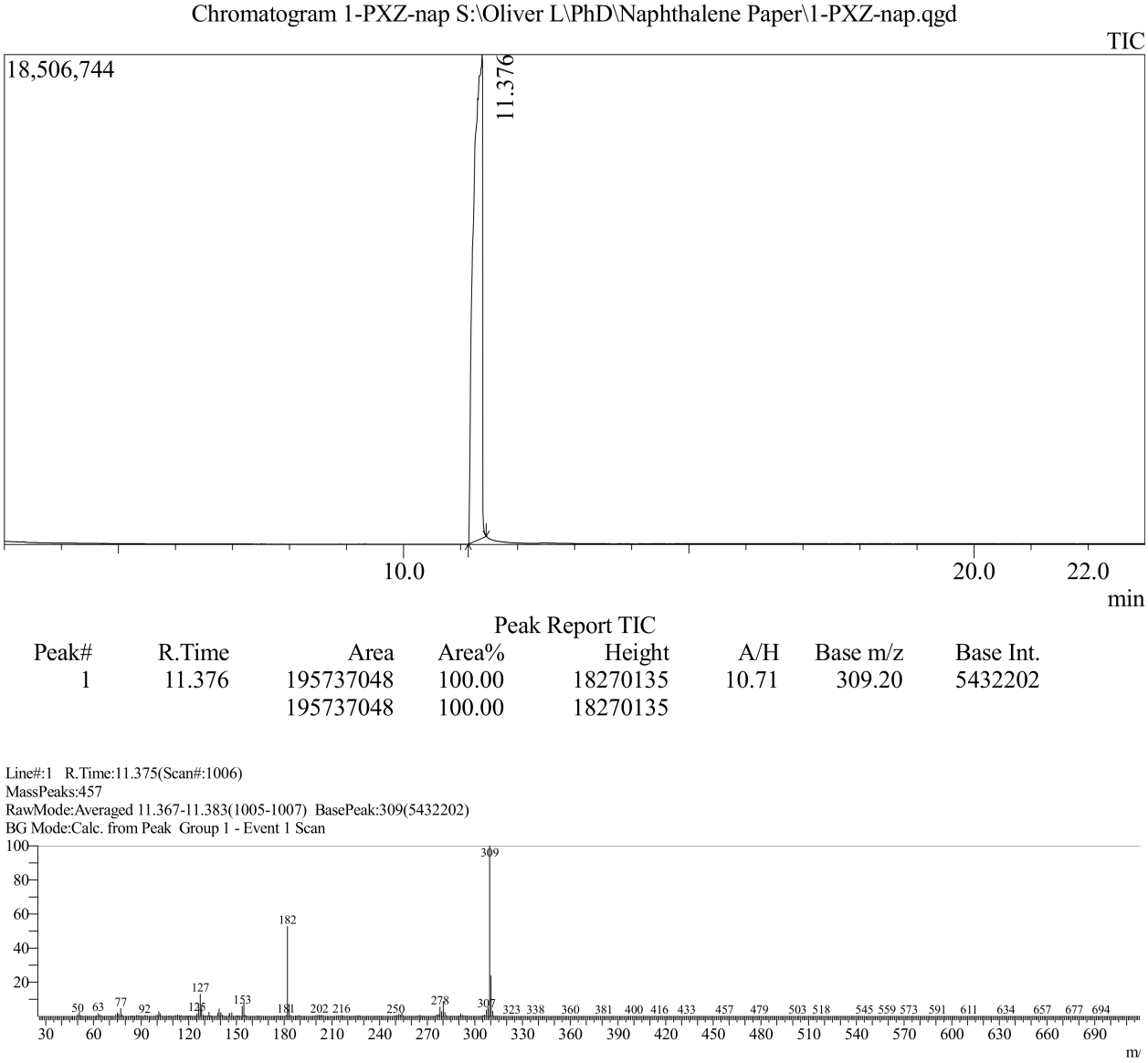

Figure **S13**. GCMS of **1-PXZ-Nap**

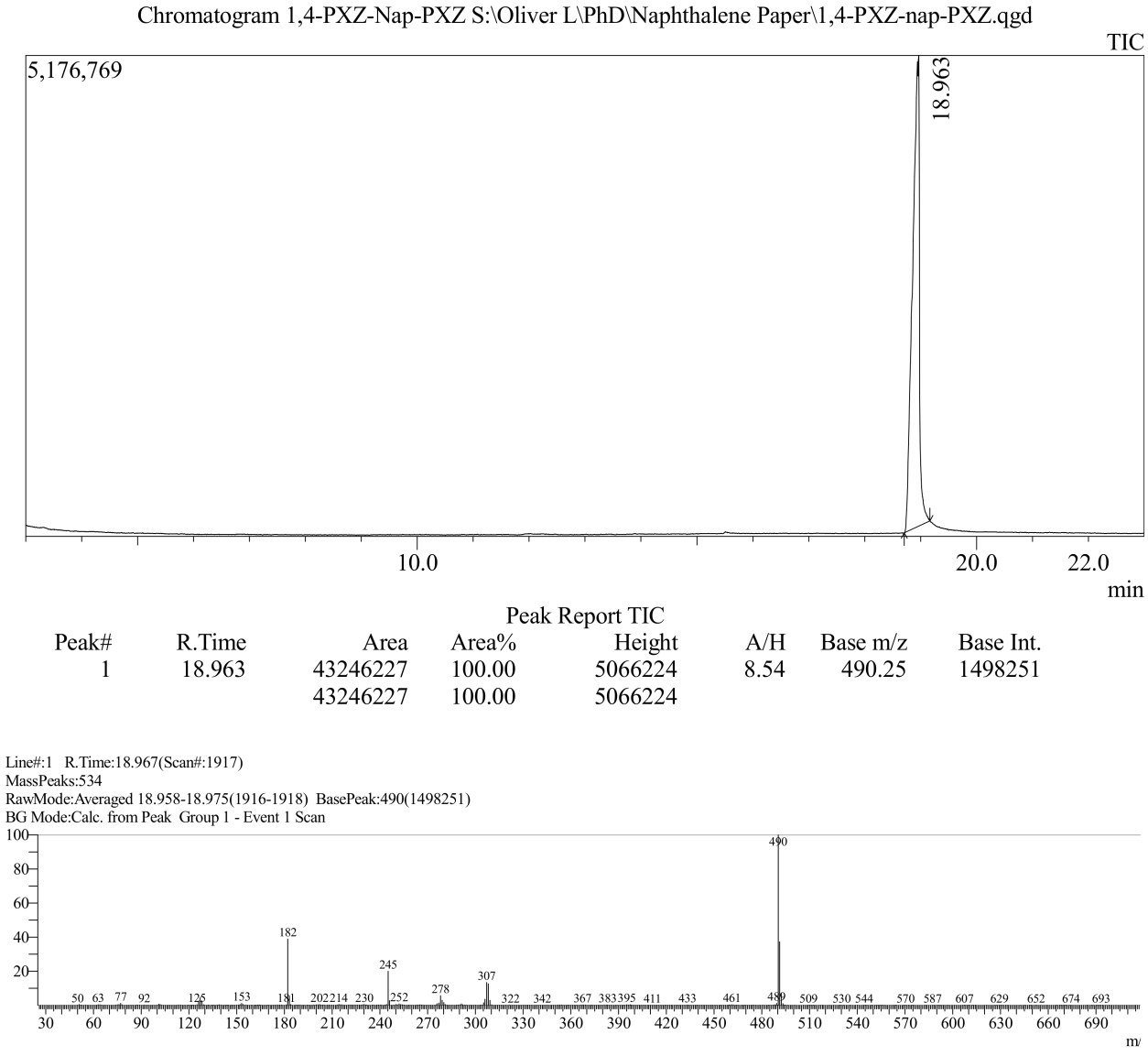

Figure **S14**. GCMS of **1,4-PXZ-Nap-PXZ**

8 Crystal Structures

In all cases, neutral atom scattering factors were taken from International Tables for Crystallography (IT), Vol. C, Table 6.1.1.4[24]. Anomalous dispersion effects were included in Fcalc[25]; the values for Δf' and Δf'' were those of Creagh and McAuley.[26] The values for the mass attenuation coefficients are those of Creagh and Hubbell.[27] All calculations were performed using the CrystalStructure[28] crystallographic software package except for refinement, which was performed using SHELXL Version 2018/3.[29]

Least Squares function minimized: (SHELXL Version 2018/3)

$\Sigma w(F_o^2-F_c^2)^2$ where w = Least Squares weights.

Goodness of fit is defined as:

$[\Sigma w(F_o^2-F_c^2)^2/(N_o-N_v)]^{1/2}$

where: N_o = number of observations

N_v = number of variables

The crystallographic data has been deposited with the Cambridge Crystallographic Data Centre (CCDC) with deposition numbers: 2303516 (**1-PXZ-Nap**), 2303517 (**2-PXZ-Nap**), and 2303518 (**1,4-PXZ-Nap-PXZ**).

8.1 2-PXZ-Nap

A colorless plate crystal of $C_{22}H_{15}NO$ having approximate dimensions of 0.200 x 0.100 x 0.010 mm was mounted in a loop. All measurements were made on a Rigaku XtaLAB P200 diffractometer using multi-layer mirror monochromated Mo-Kα radiation. Cell constants and an orientation matrix for data collection corresponded to a primitive monoclinic cell with dimensions:

a = 6.1593(16) Å

b = 23.215(7) Å β = 105.9870(10)°

c = 11.123(4) Å

V = 1528.9(8) Å^3

For Z = 4 and F.W. = 309.37, the calculated density is 1.344 g/cm^3. The reflection conditions of:

h0l: l = 2n

0k0: k = 2n

uniquely determine the space group to be:

$P2_1/c$ (#14)

The data were collected at a temperature of -100 ± 1°C to a maximum 2θ value of 50.8°. Of the 10984 reflections were collected, where 2784 were unique (R_{int} = 0.0226); equivalent reflections were merged. Data were collected and processed using CrystalClear (Rigaku).[30] The linear absorption coefficient, μ, for Mo-Kα radiation is 0.822 cm^{-1}. An empirical absorption correction was applied which resulted in transmission factors ranging from 0.861 to 0.999. The data were corrected for Lorentz and polarization effects. The structure was solved by direct methods[31] and expanded using Fourier techniques. The non-hydrogen atoms were refined anisotropically. Hydrogen atoms were refined using the riding model. The final cycle of full-matrix least-squares refinement on F^2 was based on 2784 observed reflections and 217 variable parameters and converged (largest parameter shift was 0.00 times its esd) with unweighted and weighted agreement factors of:

$R1 = \Sigma \, ||Fo| - |Fc|| \, / \, \Sigma \, |Fo| = 0.0417$

$wR2 = [\Sigma (w (Fo^2 - Fc^2)^2) / \Sigma \, w(Fo^2)^2]^{1/2} = 0.1224$

The goodness of fit was 1.04. Unit weights were used. The maximum and minimum peaks on the final difference Fourier map corresponded to 0.44 and -0.20 $e^-/Å^3$, respectively.

8.2 1-PXZ-Nap

A colourless prism crystal of $C_{22}H_{15}NO$ having approximate dimensions of 0.200 x 0.200 x 0.200 mm was mounted in a loop. All measurements were made on a Rigaku XtaLAB P100 diffractometer using multi-layer mirror monochromated Cu-Kα radiation. Cell constants and an orientation matrix for data collection corresponded to a primitive triclinic cell with dimensions:

a = 8.7284(7) Å α = 110.237(6)°

b = 9.2222(7) Å β = 100.707(6)°

c = 11.3466(7) Å γ = 108.806(7)°

V = 764.42(12) $Å^3$

For Z = 2 and F.W. = 309.37, the calculated density is 1.344 g/cm^3. Based on a statistical analysis of intensity distribution, and the successful solution and refinement of the structure, the space group was determined to be:

P-1 (#2)

The data were collected at a temperature of -100 ± 1°C to a maximum 2θ value of 134.1°. Of the 6908 reflections were collected, where 2684 were unique (R_{int} = 0.0521). Data were collected and processed using CrysAlisPro (Rigaku Oxford Diffraction).[32] The linear absorption coefficient, μ, for Cu-Kα radiation is 6.455 cm^{-1}. An empirical absorption correction was applied which resulted in transmission factors ranging from 0.678 to 0.879. The data were corrected for Lorentz and polarization effects. A correction for secondary extinction[33] was applied (coefficient = 0.096970). The structure was solved by direct methods[31] and expanded using Fourier techniques. The non-hydrogen atoms were refined anisotropically. Hydrogen atoms were refined using the riding model. The final cycle of full-matrix least-squares refinement on F^2 was based on 2684 observed reflections and 218 variable parameters and converged (largest parameter shift was 0.00 times its esd) with unweighted and weighted agreement factors of:

$R1 = \Sigma \, ||Fo| - |Fc|| \, / \, \Sigma \, |Fo| = 0.1110$

$wR2 = [\Sigma (w (Fo^2 – Fc^2)^2) / \Sigma \, w(Fo^2)^2]^{1/2} = 0.3259$

The goodness of fit was 1.63. Unit weights were used. The maximum and minimum peaks on the final difference Fourier map corresponded to 0.67 and -0.68 $e^-/Å^3$, respectively.

8.3 1,4-PXZ-Nap-PXZ

A yellow prism crystal of $C_{34}H_{22}N_2O_2$ having approximate dimensions of 0.040 x 0.040 x 0.040 mm was mounted in a loop. All measurements were made on a Rigaku XtaLAB P200 diffractometer using multi-layer mirror monochromated Mo-Kα radiation. Cell constants and an orientation matrix for data collection corresponded to a primitive triclinic cell with dimensions:

a	= 9.065(4) Å	α	= 95.103(11)°
b	= 11.616(5) Å	β	= 90.394(6)°
c	= 11.685(4) Å	γ	= 102.932(12)°
V	= 1194.0(8) $Å^3$		

For Z = 2 and F.W. = 490.56, the calculated density is 1.364 g/cm^3. Based on a statistical analysis of intensity distribution, and the successful solution and refinement of the structure, the space group was determined to be:

P-1 (#2)

The data were collected at a temperature of -180 ± 1°C to a maximum 2θ value of 50.8°. Of the 13566 reflections were collected, where 4311 were unique (R_{int} = 0.0673); equivalent reflections were

merged. Data were collected and processed using CrystalClear (Rigaku).[30] The linear absorption coefficient, μ, for Mo-Kα radiation is 0.852 cm^{-1}. An empirical absorption correction was applied which resulted in transmission factors ranging from 0.603 to 0.997. The data were corrected for Lorentz and polarization effects. The structure was solved by direct methods[31] and expanded using Fourier techniques. The non-hydrogen atoms were refined anisotropically. Hydrogen atoms were refined using the riding model. The final cycle of full-matrix least-squares refinement on F^2 was based on 4311 observed reflections and 343 variable parameters and converged (largest parameter shift was 0.00 times its esd) with unweighted and weighted agreement factors of:

$R1 = \Sigma \, ||Fo| - |Fc|| \, / \, \Sigma \, |Fo| = 0.0842$

$wR2 = [\, \Sigma \, (\, w \, (Fo^2 - Fc^2)^2 \,) / \, \Sigma \, w(Fo^2)^2]^{1/2} = 0.3028$

The goodness of fit was 1.22. Unit weights were used. The maximum and minimum peaks on the final difference Fourier map corresponded to 0.59 and -0.63 $e^-/Å^3$, respectively.

9 Film Photoluminescence Quantum Yield

Table **S5**. PLQY data of doped and neat films of the three emitters.

		2-PXZ-Nap	**1-PXZ-Nap**	**1,4-PXZ-Nap-PXZ**
Neat film	Φ_{PL} (N2) /%	1.7	2.0	20.0
	Φ_{PL} (Air) /%	1.6	1.4	18.0
PMMA 10 wt %	Φ_{PL} (N2) /%	<1.0	1.6	21.6
	Φ_{PL} (Air) /%	1.5	1.4	17.8
mCP 3 wt%	Φ_{PL} (N2) /%	5.5	9.0	NR
	Φ_{PL} (Air) /%	3.0	2.0	NR
mCP 5 wt%	Φ_{PL} (N2) /%	7.0	8.1	35.8
	Φ_{PL} (Air) /%	3.3	2.3	4.2
mCP 10 wt%	Φ_{PL} (N2) /%	6.6	7.0	31.5
	Φ_{PL} (Air) /%	1.6	1.8	6.9
mCP 15 wt%	Φ_{PL} (N2) /%	5.3	4.6	31.4
	Φ_{PL} (Air) /%	1.2	1.9	7.0
mCP 20 wt%	Φ_{PL} (N2) /%	NR	NR	48.0
	Φ_{PL} (Air) /%	NR	NR	7.0

NR: Not recorded.

10 Organic Light-Emitting Diode Fabrication

The OLED devices were fabricated in a bottom emitting architecture via vacuum sublimation under high vacuum at a base pressure of 2-5×10^{-7} mbar. The organic layer sequence and the metal cathode were deposited onto pre-cleaned glass substrates coated with indium tin oxide (ITO) which has a sheet resistance of around 30 Ω/sq. A pre-patterned ITO glass substrate was treated by ultrasonic cleaning in acetone and isopropanol consecutively and then treated by oxygen plasma before the transfer to the vacuum chamber. Organic layers were deposited at a rate of 0.3-0.6 Å/s, which was controlled in-situ using quartz crystal monitors. Doping of the emission layers was achieved through co-evaporation of the emitter and host materials. The electron injection layer, LiF, was deposited at a rate of 0.10 Å/s, while the Al cathode was deposited at a rate of 0.5 Å/s through the shadow mask defining the top electrode. The spatial overlap of the anode and cathode electrodes determined the active area of the OLED which was estimated to be 2 mm^2. All the devices were encapsulated with glass lids and UV epoxy resin inside the inert atmosphere. The luminance-current-voltage characteristics were measured in an ambient environment using a Keithley 2400 source meter and Keithley 2000 multimeter connected to a calibrated Si photodiode. The external quantum efficiency was calculated assuming Lambertian emission distribution. The electroluminescence spectra were recorded by an Andor DV420-BV CCD spectrometer.

11 Low Temperature Solution PL

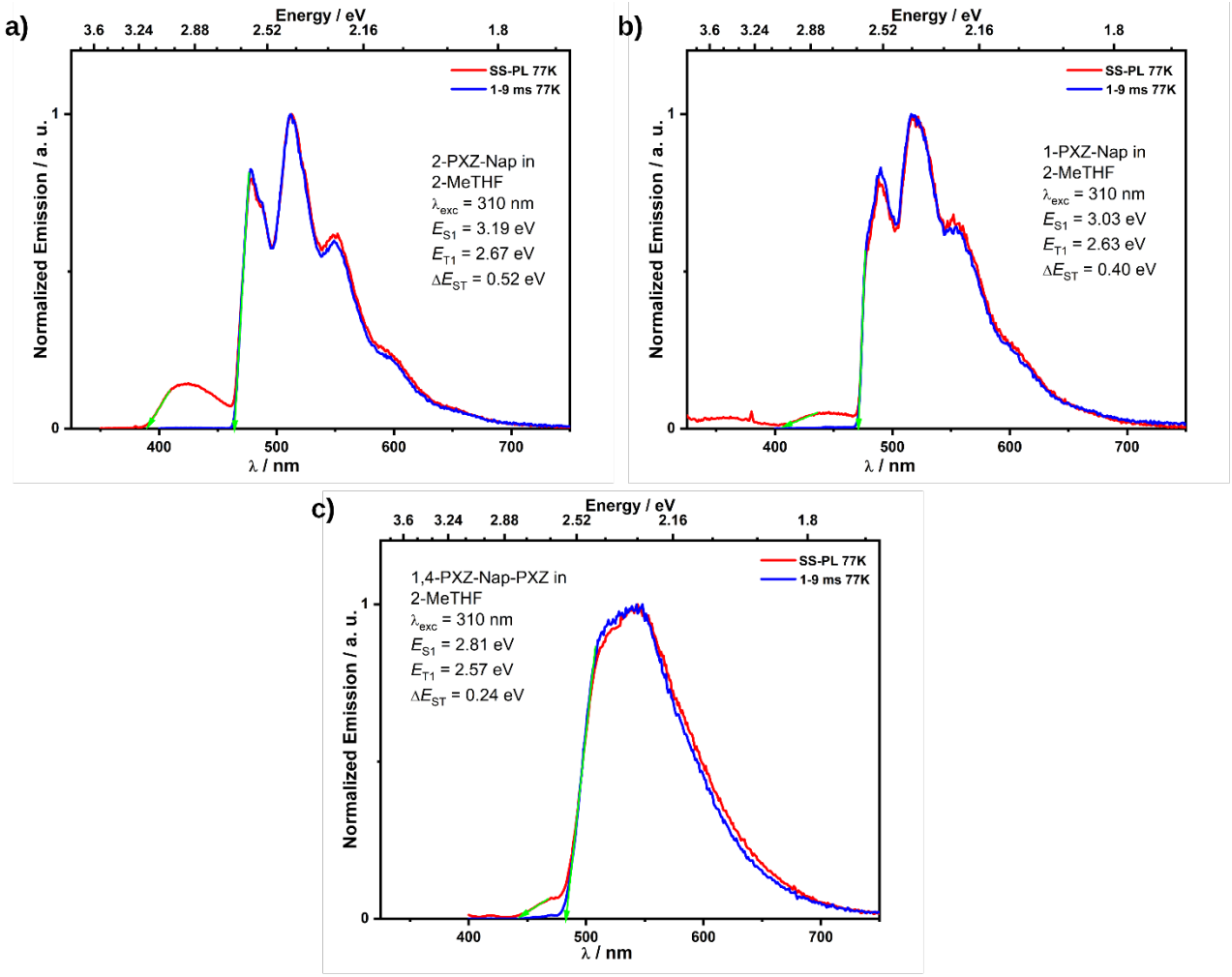

Figure **S15**. Steady-state (red) and time-gated (1-9 ms, blue) emission in 2-methyltetrahydrofuran at 77 K. a) 2-PXZ-Nap. b) 1-PXZ-Nap. c) 1,4-PXZ-Nap-PXZ.

12 References

1 J. P. Perdew, K. Burke and M. Ernzerhof, *Phys. Rev. Lett.*, 1996, **77**, 3865–3868.
2 J. P. Perdew, K. Burke and M. Ernzerhof, *Phys. Rev. Lett.*, 1997, **78**, 1396–1396.
3 C. Adamo and V. Barone, *J. Chem. Phys.*, 1999, **110**, 6158–6170.
4 R. Ditchfield, W. J. Hehre and J. A. Pople, *J. Chem. Phys.*, 1971, **54**, 724–728.
5 W. J. Hehre, R. Ditchfield and J. A. Pople, *J. Chem. Phys.*, 1972, **56**, 2257–2261.
6 P. C. Hariharan and J. A. Pople, *Theor. Chim. Acta*, 1973, **28**, 213–222.
7 P. C. Hariharan and J. A. Pople, *Mol. Phys.*, 1974, **27**, 209–214.
8 S. Grimme, J. Antony, S. Ehrlich and H. Krieg, *J. Chem. Phys.*, 2010, **132**, 154104.
9 S. Grimme, S. Ehrlich and L. Goerigk, *J. Comput. Chem.*, 2011, **32**, 1456–1465.
10 R. Bauernschmitt and R. Ahlrichs, *Chem. Phys. Lett.*, 1996, **256**, 454–464.
11 M. E. Casida, C. Jamorski, K. C. Casida and D. R. Salahub, *J. Chem. Phys.*, 1998, **108**, 4439–4449.
12 R. E. Stratmann, G. E. Scuseria and M. J. Frisch, *J. Chem. Phys.*, 1998, **109**, 8218–8224.
13 S. Hirata and M. Head-Gordon, *Chem. Phys. Lett.*, 1999, **314**, 291–299.
14 M. J. Frisch, G. W. Trucks, H. B. Schlegel, G. E. Scuseria, M. A. Robb, J. R. Cheeseman, G. Scalmani, V. Barone, G. A. Petersson, H. Nakatsuji, X. Li, M. Caricato, A. V. Marenich, J.

Bloino, B. G. Janesko, R. Gomperts, B. Mennucci, H. P. Hratchian, J. V. Ortiz, A. F. Izmaylov, J. L. Sonnenberg, D. Williams-Young, F. Ding, F. Lipparini, F. Egidi, J. Goings, B. Peng, A. Petrone, T. Henderson, D. Ranasinghe, V. G. Zakrzewski, J. Gao, N. Rega, G. Zheng, W. Liang, M. Hada, M. Ehara, K. Toyota, R. Fukuda, J. Hasegawa, M. Ishida, T. Nakajima, Y. Honda, O. Kitao, H. Nakai, T. Vreven, K. Throssell, J. A. Montgomery Jr., J. E. Peralta, F. Ogliaro, M. J. Bearpark, J. J. Heyd, E. N. Brothers, K. N. Kudin, V. N. Staroverov, T. A. Keith, R. Kobayashi, J. Normand, K. Raghavachari, A. P. Rendell, J. C. Burant, S. S. Iyengar, J. Tomasi, M. Cossi, J. M. Millam, M. Klene, C. Adamo, R. Cammi, J. W. Ochterski, R. L. Martin, K. Morokuma, O. Farkas, J. B. Foresman and D. J. Fox, Gaussian 16, Revision C.01 2016.

15 O. S. Lee and E. Zysman-Colman, Silico (version 0.18) 2020.

16 N. M. O'Boyle, A. L. Tenderholt and K. M. Langner, *J. Comput. Chem.*, 2008, **29**, 839–845.

17 W. Humphrey, A. Dalke and K. Schulten, *J. Mol. Graph.*, 1996, **14**, 33–38.

18 J. Stone, Computer Science Department, University of Missouri-Rolla, 1998.

19 J. D. Hunter, *Comput. Sci. Eng.*, 2007, **9**, 90–95.

20 N. M. O'Boyle, M. Banck, C. A. James, C. Morley, T. Vandermeersch and G. R. Hutchison, *J. Cheminformatics*, 2011, **3**, 33.

21 N. M. O'Boyle, C. Morley and G. R. Hutchison, *Chem. Cent. J.*, 2008, **2**, 5.

22 N. G. Connelly and W. E. Geiger, *Chem. Rev.*, 1996, **96**, 877–910.

23 G. A. Crosby and J. N. Demas, *J. Phys. Chem.*, 1971, **75**, 991–1024.

24 In *International Tables for Crystallography*, Kluwer Academic Publishers, Dordrecht, Netherlands, 1992, vol. C, p. 572.

25 J. A. Ibers and W. C. Hamilton, *Acta Crystallogr.*, 1964, **17**, 781–782.

26 D. C. Creagh and W. J. McAuley, in *International Tables for Crystallography*, Kluwer Academic Publishers, Dordrecht, Netherlands, 1992, vol. C, pp. 219–222.

27 D. C. Creagh and J. H. Hubbell, in *International Tables for Crystallography*, Kluwer Academic Publishers, Dordrecht, Netherlands, 1992, vol. C, pp. 200–206.

28 CrystalStructure 4.3: Crystal Structure Analysis Package Rigaku Corporation, Tokyo 196-8666, Japan. 2000.

29 G. M. Sheldrick, *Acta Crystallogr. A*, 2008, **A64**, 112–122.

30 CrystalClear: Data Collection and Processing Software Rigaku Corporation, Tokyo 196-8666, Japan. 1998.

31 G. M. Sheldrick, *Acta Cryst*, 2014, **A70**, C1437.

32 CrysAlisPro: Data Collection and Processing Software Rigaku Corporation, Tokyo 196-8666, Japan. 2015.

33 A. Larson, *Munksgaard*, 1970, 291–294.